Photoluminescence quenching of tris-(8-hydroxyquinoline) aluminum thin films at interfaces with metal oxide films of different conductivities

Jun Mei, M. Scott Bradley, and Vladimir Bulović
Laboratory of Organic Optics and Electronics, Massachusetts Institute of Technology, Cambridge, Massachusetts 02139, USA
(Received 1 March 2009; revised manuscript received 13 May 2009; published 10 June 2009)

We report a comprehensive study of photoluminescence (PL) quenching of tris-(8-hydroxyquinoline) aluminum (Alq_3) at interfaces with thin films of tin oxide (SnO_2) using both steady-state and time-resolved measurements. Quenching of excitons generated in the Alq_3 layer increased with increased conductivity of the SnO_2 films, which we relate with the presence of nonradiative energy transfer from excitons in Alq_3 to transitions in SnO_2. In addition, due to the semitransparency of SnO_2, the effects of optical interference on the steady-state PL quenching of Alq_3 are determined. We demonstrate that without accounting for the interference effects in the excitation, the extracted exciton diffusion length (L_d) in Alq_3 is in the range of 10–20 nm. However, when using a numerical model to account for the optical interference effects, we find that L_d is in the range of 5–9 nm, which agrees with L_d extracted from time-resolved measurements (4–6 nm). We conclude that time-resolved measurements are least affected by optical interference, yielding the most accurate measurement of L_d.

DOI: 10.1103/PhysRevB.79.235205 PACS number(s): 71.35.Aa, 78.55.Kz, 78.20.−e

I. INTRODUCTION

Metal oxide thin films have long been used as transparent electrodes in organic optoelectronic devices, but their interaction with excitons in their neighboring organic thin films has seldom been investigated. For example, despite numerous studies of photoluminescence (PL) quenching of organic dyes at interfaces with metallic films, there has not yet been a comprehensive study on PL quenching of excitons in organic films at interfaces with metal oxide layers.[1–10] Exciton quenching at the interfaces of organic films is manifested in measurements of the exciton diffusion length (L_d),[11] which in this study we measure for evaporated thin films of tris-(8-hydroxyquinoline) aluminum (Alq_3) on top of tin-oxide (SnO_2)-coated glass. The Alq_3 exciton diffusion length reported in literature varies widely, from 5 to 30 nm, at room temperature.[7,8,12–18] In this study, we find that the variation can be attributed to the optical interference in the PL measurements and that the true L_d in Alq_3 thin films is 6 ± 2 nm. To determine L_d, we measured the PL efficiency of Alq_3 films of different thicknesses on the top of the quenching Alq_3/SnO_2 interface. Additionally, variation in conductivity of the quenching layer, and therefore the variation in the quenching layer's absorption coefficient, allows for the presence of nonradiative energy transfer from Alq_3 to SnO_2 to be probed directly.

II. EXPERIMENT

A. Sample fabrication

Samples were fabricated on clean glass substrates, which were cut from 1-mm-thick electroverre glass sheets manufactured by Erie Scientific Co. SnO_2 films were deposited via radio-frequency sputtering (sputtering target, 99.99% pure, was made by AJA International). The sputtering chamber was evacuated below 5×10^{-7} Torr prior to SnO_2 deposition. A mixture of argon (Ar) and oxygen (O_2) was used as the plasma-forming gas. Films of different oxygen contents were deposited by varying the oxygen flow rate while fixing the total flow rate at 10 SCCM (SCCM denotes cubic centimeter per minute at STP) and the total pressure at 3 mTorr. Film thickness and deposition rate were monitored using a Sycon STM-100/MF, and the deposition rate was maintained for all samples between 1.3 and 1.5 Å/s. For some samples, as indicated in the text, prior to Alq_3 thin-film deposition a self-assembled monolayer (SAM) was applied to SnO_2 and glass surfaces using 3-aminopropyltriethoxysilane (APTES) as a precursor, manufactured by Pierce Biotechnology, Inc. The following procedure was used: mix 2% APTES with 93% ethanol and 5% de-ionized water by volume; adjust the *p*H with acetic acid to 4.5–5.5; immerse clean oxide substrates in the mixture for one and a half minutes; rinse substrates in ethanol and blow dry with nitrogen; finally, heat substrates at 100 °C for 10 min. To confirm that a uniform SAM had been coated on the oxide surface, we made contact-angle measurements confirming that the surface is hydrophobic and used atomic force microscopy to characterize the surface morphology. The thickness of the monolayer was measured by a Geartner ellipsometer model L126B. Alq_3 (from TCI) was purified using ultrahigh vacuum thermal-gradient sublimation prior to deposition. Alq_3 films were evaporated onto the substrates via Joule heating in vacuum ($<7.0 \times 10^{-7}$ Torr). The deposition rate was maintained the same for all samples in a range of 1.2–1.6 Å/s. Completed samples were stored in a nitrogen environment at room temperature with O_2 and moisture levels maintained below 1.0 ppm.

B. Measurements

For steady-state PL measurements, we used a Coherent Vioflame diode laser (peak wavelength $\lambda = 408$ nm, 4 mW continuous power) as an excitation source. To avoid photooxidation of organic films, a custom sample chamber had

been constructed such that completed samples could be placed in an airtight nitrogen environment for PL measurements without atmospheric exposure. PL emission was collected via an optical fiber and analyzed with a spectrometer (SpectraPro 300i by Acton Research). The custom sample chamber holds several samples, allowing for multiple PL measurements without changing the alignment of the setup, ensuring consistent input intensity from sample to sample. Time-resolved measurements were carried out using a $\lambda = 395$ nm pulse excitation source (pulse width <200 fs) powered by a Coherent Mira 900F mode-locked Ti:sapphire laser. The input intensity was modulated with a Coherent RegA 9000 regenerative amplifier. A repetition rate of 100 kHz was used for all measurements. Emitted photons were collected and analyzed using a Hamamatsu C4780 picosecond fluorescence lifetime system consisting of a Hamamatsu C4334 Streak Camera and a C5094 spectrograph. All of the measurements were integrated over 200 000 frames at a frame capture rate of 60 Hz and with a time window of 100 ns. The intensity vs time profile was obtained by integrating the Alq_3 emission spectrum from $\lambda = 480$ nm to $\lambda = 580$ nm.

Optical transmittance and reflectance measurements were performed on an Aquila nkd-8000. For Hall-effect measurements, we used a Keithley 2600 as a current source and an electromagnet to provide a magnetic-field intensity of up to 4.4 ± 0.1 kG.

III. THEORY

Given a number of concurrent and independent processes such as exciton generation, diffusion, and decay, Burin and Ratner[15] proposed that the exciton population density N at any position $\mathbf{r}$ and time t in an organic thin film with a quenching interface at $x=0$ can be described by

$$\frac{\partial N}{\partial t} = D\frac{\partial^2 N}{\partial \mathbf{r}^2} - \frac{N}{\tau_0}\left[1 + \left(\frac{x_0}{x}\right)^3\right] + G \tag{1}$$

with x as the distance from the quenching interface into the organic thin film and D, τ_0, x_0, and G are defined below.

In this model, it is assumed that excitons are generated by photoexcitation only with light incident from $x=+\infty$. Under steady-state illumination, the generation rate G is invariant with time; the distance dependence is commonly assumed to follow Beer's law, viz., $G(x) \propto \exp[\alpha(x-d)]$, where $x=d$ is the illuminated sample surface (thus $0 \le x \le d$ indicates a position within the organic film) and α is the absorption coefficient at the excitation wavelength. For films much thinner than α^{-1}, G can also be assumed to be invariant with distance. The migration of excitons is modeled by a classical nondispersive diffusion process, with diffusion constant D. It is well known that nonradiative energy transfer can occur near the interface with an absorbing layer (e.g., a metal electrode),[1–10] and the rate of energy transfer has been observed to follow an inverse cubic law with distance.[1,2] Thus, the total exciton decay rate τ^{-1} is formulated as

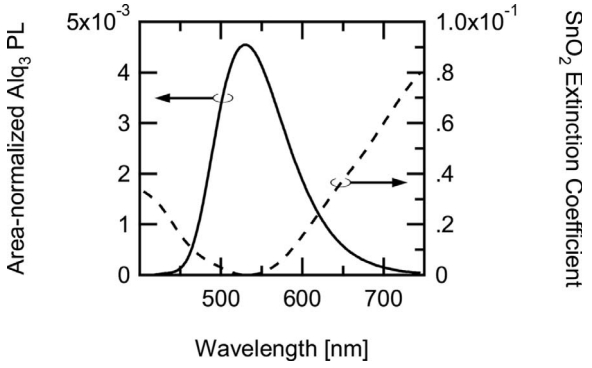

FIG. 1. The overlap between the measured emission spectrum of Alq_3 and the reported extinction coefficient of SnO_2 (Ref. 20).

$$\frac{1}{\tau} = \frac{1}{\tau_0}\left[1 + \left(\frac{x_0}{x}\right)^3\right], \tag{2}$$

where τ_0^{-1} is the total decay rate in the absence of the absorbing layer and x_0 is the distance at which the probability that an exciton decays by nonradiative energy transfer to the quenching layer is 1/2. A general expression for x_0 is given by[9]

$$x_0^3 = \frac{3\phi}{32}\frac{\lambda^3\Theta}{\pi^3 n_1}\left[\frac{n_2\kappa_2}{(n_1^2 + n_2^2 - \kappa_2^2)^2 + 4n_2^2\kappa_2^2}\right], \tag{3}$$

where λ is the emission wavelength, ϕ is the luminescent yield, n_1 is the real part of the refractive index of the host medium, n_2 and κ_2 are the real and imaginary parts of the complex refractive index of the quenching medium, and Θ is a geometry factor for different dipole orientations with respect to the quenching layer, viz., $\Theta=2$ for a vertical dipole and 1 for a horizontal dipole. But for broad emission materials such as Alq_3, Eq. (3) should be recast in a fashion that integrates over the entire spectrum,

$$x_0^3 = \frac{3\phi}{32}\frac{\Theta}{\pi^3}\int_0^\infty \frac{n_2\kappa_2 f(\lambda)}{(n_1^2 + n_2^2 - \kappa_2^2)^2 + 4n_2^2\kappa_2^2}\frac{\lambda^3}{n_1}d\lambda, \tag{4}$$

where $f(\lambda)$ is the area-normalized emission spectrum of the host.

To estimate the extent of energy transfer from Alq_3 to SnO_2 with Eq. (4), we assume that the real refractive index of Alq_3 is $n=1.70$ and constant over its emission spectrum.[19] We use the area-normalized emission spectrum $f(\lambda)$ as determined by our measurements. The complex refractive index of pure SnO_2 used is that reported by Martín-Palma and Martínez-Duart.[20] The PL yield used is $\phi=0.32$,[12] and we set $\Theta=4/3$ as for a randomly orientated dipole.[9] The overlap between the Alq_3 emission and the SnO_2 extinction coefficient is plotted in Fig. 1. Integrating Eq. (4) for λ from 400 to 800 nm, we find that $x_0 \approx 32$ Å.

In the steady state, Eq. (1) is set to 0 and can be rewritten as

$$\frac{d^2N}{dx^2} - \frac{N}{L_d^2}\left(1 + \frac{x_0^3}{x^3}\right) + G' = 0, \tag{5}$$

where $L_d = \sqrt{D\tau_0}$ is the exciton diffusion length. We note that a more precise definition has that $L_d = \sqrt{ZD\tau_0}$, where $Z=2$ for strictly one-dimensional diffusion, 4 for two-dimensional diffusion, and 6 for three-dimensional diffusion.[13] But in literature, Z is usually taken as unity.[8,15–17,21,22] Therefore, we follow the same convention for direct comparison.

We evaluate the numerical solution by considering three boundary conditions: (1) no surface quenching, (2) partial quenching, and (3) complete quenching. If surface quenching does not occur, then the net flow of excitons to the interface is zero, viz., $\frac{dN}{dx}=0$. This condition also applies to the inert air/organic interface. For a partial quenching condition, the net flow of excitons to the quenching interface is balanced by the rate at which excitons are quenched, viz., $D\frac{dN}{dx} = \upsilon N$, where υ is the quenching velocity. If υ is large, then the interface becomes a perfect quencher, and the exciton population density at the quenching surface is always zero. From the solution to Eq. (1), the PL quantum efficiency can be obtained by finding the rates of absorption (A) and emission (F)

$$A(w) = \int_0^w G dx, \quad F(w) = \int_0^w \frac{N}{\tau_r} dx, \tag{6}$$

where $\tau_r^{-1} = \phi\tau_0^{-1}$ is the radiative decay rate. Thus, the PL efficiency for a film of thickness w is $\phi(w) = F(w)/A(w)$.

IV. RESULTS AND DISCUSSION

A. Photoluminescence quenching by SnO_2

In Fig. 2, we show PL quenching of a series of thin films of Alq_3 by SnO_2 through steady-state PL measurements with varying Alq_3 thickness. Figure 2(a) shows that the normalized emission spectra peak at $\lambda = 523 \pm 3$ nm. Relative peak intensity of each sample is plotted in Fig. 2(c), which shows a significant decrease in the photoluminescence of Alq_3 with thickness. We also observe similar quenching effects from time-resolved measurements (Fig. 3), which show that the average exciton decay rate increases with decreasing Alq_3 thickness.

In subsequent analysis, we consider two most likely external quenching mechanisms: (1) surface quenching at the Alq_3/SnO_2 interface and (2) nonradiative energy transfer to SnO_2 transitions. The former can occur at type II heterointerfaces for which the band offset is greater than the exciton binding energy. In this case, excitons in Alq_3 can dissociate into separate charge carriers upon arrival at the Alq_3/SnO_2 interface, as illustrated in Fig. 4(a). Alternatively, dangling bonds at the SnO_2 surface could result in formation of midgap states that could act as recombination sites for Alq_3 excitons. The efficiency of this process depends on the energy levels and the contact between the two layers. Nonradiative energy transfer can become significant if there is a sufficiently large spectral overlap between the absorption spectrum of the quencher and the emission spectrum of Alq_3, as in the case with a metallic electrode.[1–10] Below, we demonstrate that Alq_3 can energy transfer to SnO_2, as illustrated in Fig. 4(b), via two experiments: (1) modifying the optical properties of sputtered SnO_2 and (2) applying a SAM to the oxide surface.

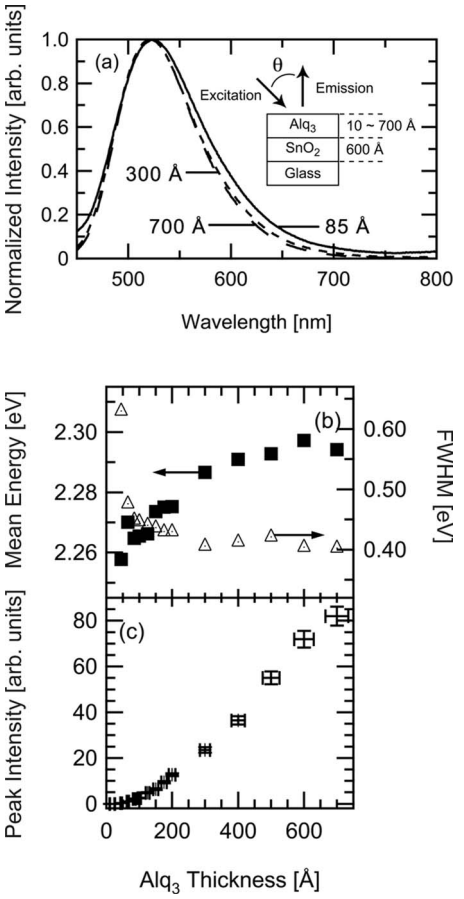

FIG. 2. Steady-state PL emission of Alq_3 with varying film thickness on 600 Å SnO_2: (a) normalized emission spectra of select samples with the sample structure illustrated in the inset, (b) mean energy and the full width at half maximum (FWHM) of the emission spectra, and (c) relative peak intensity as a function of the Alq_3 film thickness.

Optical and electrical properties of SnO_2 can be modified by tuning the film deposition conditions. In Fig. 5, we show

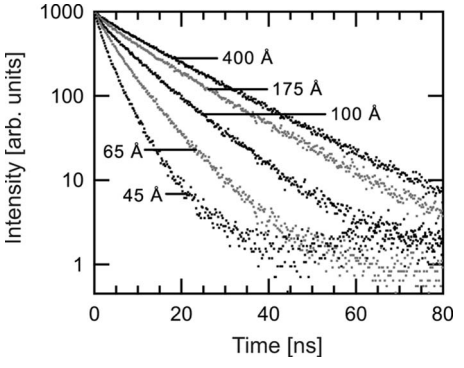

FIG. 3. Integrated time-resolved PL intensity as a function of time: average exciton decay rate increases with decreasing Alq_3 thickness.

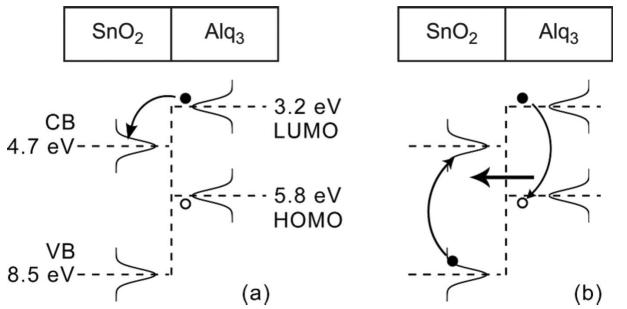

FIG. 4. Two examples by which excitons can be quenched: (a) exciton dissociation at the Alq_3/SnO_2 interface and (b) nonradiative energy transfer from Alq_3 to SnO_2. Energy levels are denoted by conduction band (CB), valence band (VB), lowest unoccupied molecular orbital (LUMO), and highest occupied molecular orbital (HOMO). Their values are obtained from literature (Refs. 23 and 24).

that as-deposited SnO_2 films become less absorptive with excess oxygen introduced into the sputtering ambient. Through ellipsometry measurements at a select wavelength, we find that there is no significant variation ($<5\%$) in the real index of refraction of SnO_2 with varying oxygen content. Consequently, only the extinction coefficient is strongly affected by the introduction of oxygen. Furthermore, the decrease in absorption with increasing oxygen content is accompanied by a decrease in the carrier density, as determined by Hall-effect measurements (Fig. 6). Thus, it is likely that excess oxygen reduces the oxygen vacancies, which are intrinsic donors,[25] in the sputtered SnO_2 films, thereby removing those energy states that are responsible for the absorption in the visible spectrum.

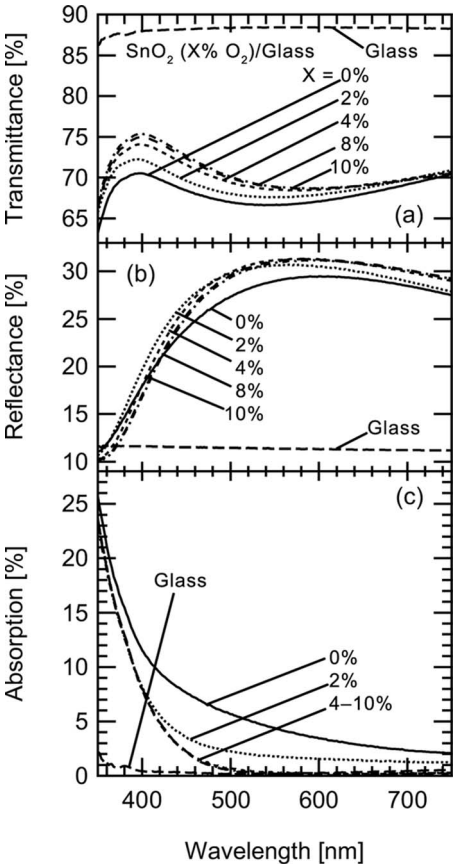

FIG. 5. Optical properties of 700 Å SnO_2 samples sputtered in different oxygen content (measured by ratio of the oxygen flow rate to the total gas flow rate): (a) transmittance, (b) reflectance, and (c) absorption.

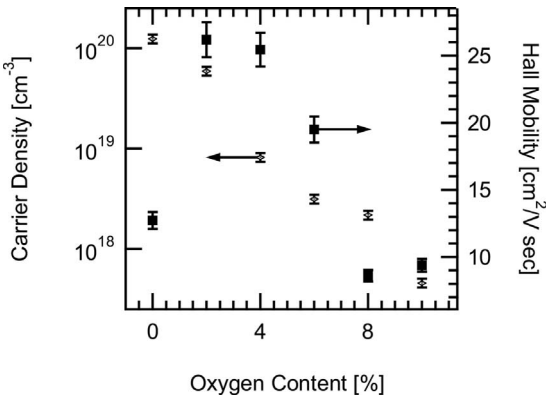

FIG. 6. Change in the carrier density and Hall mobility as a function of the oxygen content.

By measuring the steady-state PL spectra of Alq_3 on these SnO_2 films, we find that the emission intensity rises steadily with the SnO_2 oxygen content, as shown in Fig. 7(a), which indicates a reduction in PL quenching. To estimate the absorption of the Alq_3 layer, we implement a thin-film dielec-

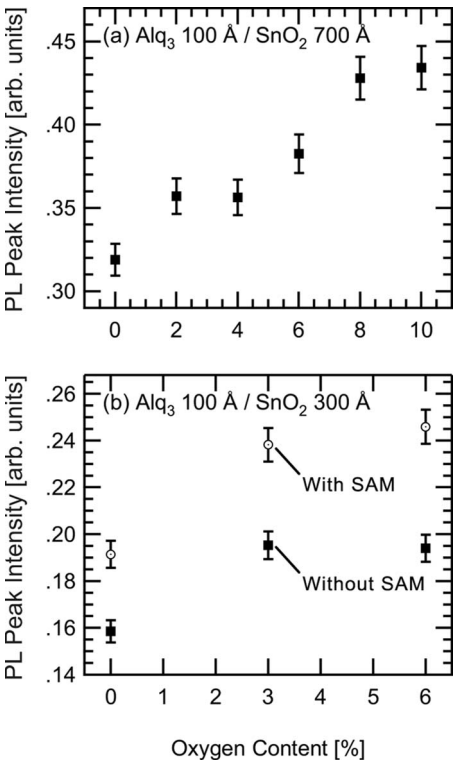

FIG. 7. Photoluminescence of 100-Å-thick Alq_3 thin film on SnO_2 substrates sputtered with different oxygen content: (a) 700-Å-thick SnO_2 films and (b) 300-Å-thick SnO_2 films with and without application of a SAM.

tric model using T matrices. Details of the model have been described elsewhere.[26] Using the refractive indices reported in literature and assuming that only the extinction coefficient of SnO_2 is reduced by excess oxygen,[19,20] we find that for all samples, the absorption in Alq_3 is 4.2%, regardless of the oxygen content. In addition, the change in reflectance at the Alq_3/SnO_2 interface calculated from the T matrices at the emission peak ($\lambda=530$ nm) is also small, rising from 8.1% for 0% O_2 to 8.6% for 6–10% O_2. Based on the T-matrix calculations, we conclude that optical interference effects on Alq_3 emission are minimal. Therefore, excess oxygen causes as-deposited SnO_2 films to be less conductive, which in turn causes SnO_2 to quench Alq_3 less effectively. Consequently, we conclude that nonradiative energy transfer from excitons in Alq_3 to transitions in SnO_2 plays a major role in the quenching of Alq_3 photoluminescence.

In a second experiment, we applied a SAM to the oxide surface. Ellipsometry measurements indicate that the SAM thickness is 6 ± 3 Å, with the real part of index of refraction of about 1.35 at $\lambda=633$ nm, and the extinction coefficient is negligibly small. We compare the emission intensity of Alq_3 deposited on glass substrates with and without a SAM and confirm that the SAM does not chemically interact with Alq_3. Thus, the SAM can be used to minimize surface quenching if there is any.

We measure the steady-state PL spectra of Alq_3 deposited on SnO_2 with and without a SAM and find that the PL efficiency improves with the application of a SAM [Fig. 7(b)]. Assuming that the real part of the index of refraction of the SAM is 1.35 over the visible spectrum, T-matrix modeling indicates that introducing a SAM does not affect either the Alq_3 absorption or the reflectance at the Alq_3/SnO_2 interface. The SAM layer, therefore, may passivate the quenching midgap states at the Alq_3/SnO_2 interface, separate the excitons generated in Alq_3 from the interface where dissociation would occur, and/or reduce the rate of exciton energy transfer from Alq_3 to SnO_2 by increasing the distance between the two layers. From a device perspective, these results indicate that the exciton-generation layer, either in a light-emitting device (LED) or photodetector/photovoltaic, should be sufficiently separated from conductive metal oxide layers, especially those with significant carrier concentrations, a design consideration that was recognized in the recent demonstration of the first all inorganic colloidal quantum-dot LEDs.[27]

B. Optical interference effects

One important phenomenon that earlier studies have often overlooked is the effect of optical interference on the excitation intensity. In the following experiment, we measured the steady-state PL spectrum of 100-Å-thick Alq_3 deposited on SnO_2 with varying SnO_2 thickness. Under identical deposition conditions, these samples should not exhibit different PL yields, but we observe that the emission intensity of Alq_3 oscillates with the thickness of SnO_2 (Fig. 8). Similar effects have also been reported by Becker *et al.*[4]

Figure 8(c) shows that the Alq_3 absorption, predicted by the T matrices, oscillates in phase with the emission, but the ratio of maximum to minimum absorption is still smaller

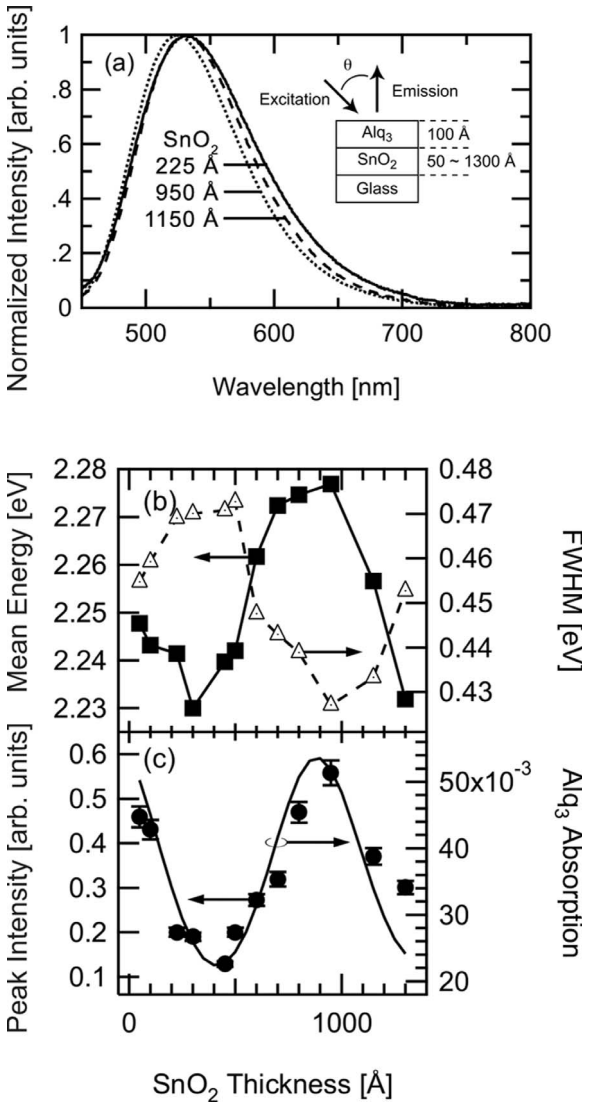

FIG. 8. Effects of the SnO_2 thickness on the emission of Alq_3: (a) steady-state PL spectra of select samples, which indicate a small but noticeable amount of spectral shift, (b) mean energy and the FWHM, both of which oscillate with the thickness of SnO_2, and (c) relative peak intensity as a function of the thickness of SnO_2. The sample structure is shown in the inset of (a). Superimposed on (c) is the Alq_3 absorption as a function of the thickness of SnO_2 predicted by the T matrices.

than that of the emission by about a factor of 2. This discrepancy may be due to averaging in the T-matrix simulation of glass thicknesses to compensate for variations in interference from the back face of the glass substrate. The considerably smaller spot size of laser excitation versus that of the spectrometer used for reflectance and transmittance measurements may mean that a more limited range of thicknesses should be averaged when simulating the absorption of laser excitation. Additionally, in Figs. 8(a) and 8(b), we note that not only the absorption but also the emission of Alq_3 can be affected by the varying SnO_2 thickness, as the 950 Å sample is blueshifted from the 225 Å sample by about 7 nm. Whereas this spectral shift is indicative of a microcavity effect on the emission[28] because the shift is relatively small,

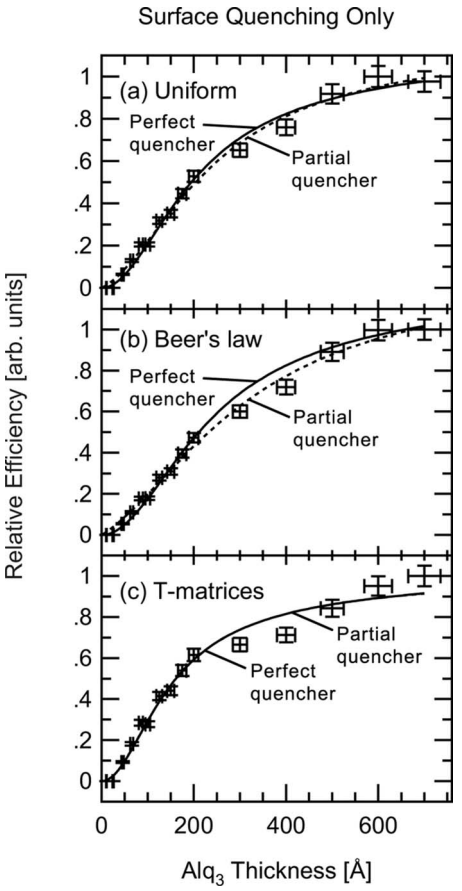

FIG. 9. Theoretical fit to the steady-state PL efficiency using the surface-quenching models. Relative absorption is approximated by (a) uniform absorption, (b) Beer's law, and (c) T matrices.

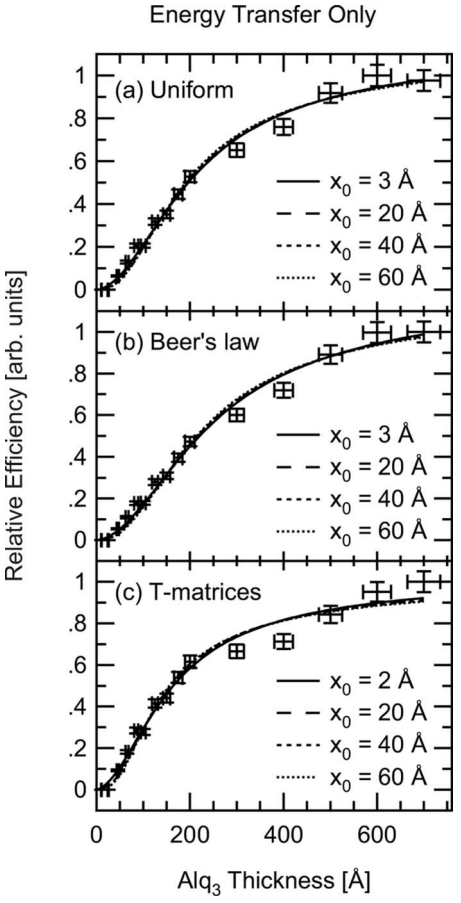

FIG. 10. Theoretical fit to the steady-state PL efficiency using the energy transfer only model. Relative absorption is approximated by (a) uniform absorption, (b) Beer's law, and (c) T matrices.

this microcavity effect is too weak to induce a large variation in the luminescence extraction efficiency.

C. Extraction of the exciton diffusion length

We extract the exciton diffusion length from steady-state and time-resolved measurements using the models described in Sec. III. In Figs. 9 and 10, we compare the relative PL efficiency from Fig. 2(c) calculated with and without any interference correction. Supposing that these samples do not exhibit strong interference effects, the generation term can be approximated by either a uniform absorption rate or by Beer's law.[29] Conversely, for the case in which optical interference is assumed to play a significant role, a correction factor is estimated for the absorption using the T-matrix simulations, and excitons are assumed to be generated uniformly throughout the organic film. Key parameters for each theoretical fit are tabulated in Table I. Overall, we find that with all input parameters optimized, each model provides a good fit to the experimental results. In particular, without any optical correction, the exciton diffusion length (L_d) in Alq_3 varies from 10 to 20 nm, a range that is commonly reported in literature. With the T-matrix absorption correction, however, L_d is shortened to a range of 5–9 nm.

For the energy transfer only cases, since the energy-transfer distance (x_0) and L_d cannot both be determined independently, we extract L_d by fixing x_0 at a particular value in a range between 1 and 60 Å. We find that for small $x_0(<5$ Å), the extracted L_d approaches that from the partial quencher case. When x_0 is in the range of 5–20 Å, the energy-transfer rate near the interface becomes sufficiently fast that the exciton population at the interface is virtually zero regardless of the surface quenching velocity. Thus, the extracted L_d approaches that from the perfect quencher case. This analysis shows that for the purpose of extracting L_d alone, it is reasonable to use the energy transfer model only to obtain the upper and lower bounds.

We apply similar analysis to the time-resolved measurements. Fitting each decay profile with a single exponential function, we obtain the average exciton decay time for each sample (Fig. 11). We solve Eq. (1) by making the following assumptions: (1) the initial exciton population is uniform at $t=0$, (2) exciton generation is zero for $t>0$, and (3) excitons are quenched by energy transfer only. The extracted L_d is found to be in the range of 40–60 Å for x_0 between 40 and 5 Å. Since only the change in the emission intensity with time is relevant in time-resolved measurements, results from this analysis are less likely to be affected by optical interference in the same samples. Thus, the exciton diffusion length extracted from time-resolved measurements is more precise than that extracted from steady-state measurements. Conversely, our analysis also shows that T matrices correctly

TABLE I. Comparison of different models: without any optical correction, the exciton diffusion length (L_d) is found to be in the range of 10–20 nm; with the T matrices, L_d is found to be in the range of 5–9 nm. Other parameters are denoted by v (surface-quenching velocity) and x_0 (energy-transfer distance).

Perfect quencher		
Absorption		L_d (Å)
Uniform		122.5 ± 12.3
Beer's law[a]		139.6 ± 16.1
T matrices		88.9 ± 13.2
Partial quencher[b]		
Absorption	v (cm/s)	L_d (Å)
Uniform	641	160.3 ± 59.3
Beer's law[a]	535	218.2 ± 88.4
T matrices	4.3×10^5	88.8 ± 44.8
Energy transfer only		
Absorption	x_0 (Å)	L_d (Å)
Uniform	3	128
	20	119
	40	108
	60	88
Beer's law[a]	3	148
	20	137
	40	127
	60	109
T matrices	2	99
	20	85
	40	69
	60	42

[a]The absorption coefficient is fixed at $\alpha = 5.6 \times 10^4$ cm^{-1}.
[b]The bulk exciton decay time is fixed at $\tau_0 = 17.4$ ns (Ref. 19).

capture the interference effects by helping to establish an agreement between the steady-state and the time-resolved measurements.

V. CONCLUSIONS

In this paper, we demonstrate that surfaces of thin films of SnO_2 quench the luminescence of Alq_3 and that nonradiative energy transfer plays a major role in this process due to the dependence of quenching magnitude on the carrier concentration in SnO_2. We characterize optical interference in the excitation using the emission spectra of Alq_3 deposited on varying thicknesses of SnO_2. Finally, we compare the exciton diffusion length extracted from theoretical fittings with and without any interference correction. We show that for steady-state measurements without any interference correction, the exciton diffusion length in Alq_3 is in the range of 10–20 nm, but with the interference correction, the exciton diffusion length is shortened to a range of 5–9 nm. The latter agrees with the range derived from time-resolved measurements, which is in the range of 4–6 nm. Our study suggests that a wide range of exciton diffusion length reported in literature may have resulted from not accounting for optical interference in measured samples.

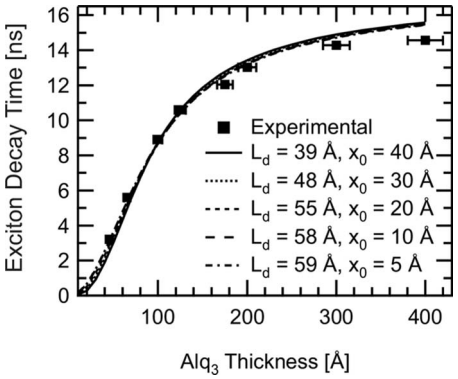

FIG. 11. The energy transfer only model provides good fits to the time-resolved measurements. The exciton diffusion length (L_d) is extracted by fixing the intrinsic decay time (τ_0) at 17.4 ns and the energy-transfer distance (x_0) at fixed values.

ACKNOWLEDGMENTS

The authors would like to thank Conor Madigan for providing the sample chamber and Steve Kooi and Polina Anikeeva for assistance in time-resolved photoluminescence measurements. This research was supported in part by the U.S. Army through the Institute for Soldier Nanotechnologies under Contract No. W911NF-07-D-0004 with the U.S. Army Research Office and the Eni Solar Frontiers Center at MIT and made use of the Shared Experimental Facilities supported in part by the MRSEC Program of the National Science Foundation under Award No. DMR 02-13282. M.S.B. acknowledges the support of the U.S. Department of Defense.

[1] G. Vaubel, H. Baessler, and D. Möbius, Chem. Phys. Lett. **10**, 334 (1971).
[2] H. Kallmann, G. Vaubel, and H. Baessler, Phys. Status Solidi B **44**, 813 (1971).
[3] H. Kuhn, J. Chem. Phys. **53**, 101 (1970).
[4] H. Becker, S. E. Burns, and R. H. Friend, Phys. Rev. B **56**, 1893 (1997).
[5] Y. Park, V.-E. Choong, B. R. Hsieh, C. W. Tang, and Y. Gao,

Phys. Rev. Lett. **78**, 3955 (1997).
[6] V.-E. Choong, Y. Park, N. Shivaparan, C. W. Tang, and Y. Gao, Appl. Phys. Lett. **71**, 1005 (1997).
[7] V.-E. Choong, Y. Park, Y. Gao, M. G. Mason, and C. W. Tang, J. Vac. Sci. Technol. A **16**, 1838 (1998).
[8] Y. Wu, Y. C. Zhou, H. R. Wu, Y. Q. Zhan, J. Zhou, S. T. Zhang, J. M. Zhao, Z. J. Wang, X. M. Ding, and X. Y. Hou, Appl. Phys. Lett. **87**, 044104 (2005).
[9] R. R. Chance, A. Prock, and R. Silbey, J. Chem. Phys. **62**, 2245 (1975).
[10] N. K. Patel, S. Cinà, and J. H. Burroughes, IEEE J. Sel. Top. Quantum Electron. **8**, 346 (2002).
[11] R. C. Powell and Z. G. Soos, J. Lumin. **11**, 1 (1975).
[12] D. Z. Garbuzov, V. Bulović, P. E. Burrows, and S. R. Forrest, Chem. Phys. Lett. **249**, 433 (1996).
[13] I. Sokolik, R. Priestley, A. D. Walser, R. Dorsinville, and C. W. Tang, Appl. Phys. Lett. **69**, 4168 (1996).
[14] R. P. Priestley, A. D. Walser, and R. Dorsinville, Opt. Commun. **158**, 93 (1998).
[15] A. L. Burin and M. A. Ratner, J. Phys. Chem. A **104**, 4704 (2000).
[16] J. Kalinowski, V. Fattori, and P. Di Marco, Chem. Phys. **266**, 85 (2001).
[17] C. L. Yang, Z. K. Tang, W. K. Ge, J. N. Wanga, Z. L. Zhang, and X. Y. Jian, Appl. Phys. Lett. **83**, 1737 (2003).
[18] J. Mężyk, J. Kalinowsky, F. Meinardi, and R. Tubino, Chem. Phys. Lett. **395**, 321 (2004).
[19] C. F. Madigan and V. Bulović, Phys. Rev. Lett. **96**, 046404 (2006).
[20] R. J. Martín-Palma and J. M. Martínez-Duart, J. Vac. Sci. Technol. A **16**, 409 (1998).
[21] P. Peumans, A. Yakimov, and S. R. Forrest, J. Appl. Phys. **93**, 3693 (2003).
[22] V. M. Kenkre and Y. M. Wong, Phys. Rev. B **22**, 5716 (1980).
[23] I. G. Hill, D. Milliron, J. Schwartz, and A. Kahn, Appl. Surf. Sci. **166**, 354 (2000).
[24] M. Grätzel, Nature (London) **414**, 338 (2001).
[25] B. J. Ingram, G. B. Gonzalez, D. R. Kammler, M. I. Bertoni, and T. O. Mason, J. Electroceram. **13**, 167 (2004).
[26] M. S. Bradley, J. R. Tischler, and V. Bulović, Adv. Mater. **17**, 1881 (2005).
[27] J. M. Caruge, J. E. Halpert, V. Wood, V. Bulovic, and M. G. Bawendi, Nat. Photonics **2**, 247 (2008).
[28] V. Bulović, V. B. Khalfin, G. Gu, P. E. Burrows, D. Z. Garbuzov, and S. R. Forrest, Phys. Rev. B **58**, 3730 (1998).
[29] M. Pope and C. E. Swenberg, *Electronic Processes in Organic Crystals and Polymers* (Oxford University Press, New York, 1999).